https://arabjchem.org

ScientificScholar®
Knowledge is power
Publisher of Scientific Journals

Arabian Journal of Chemistry

2025 18 (3) 2832024

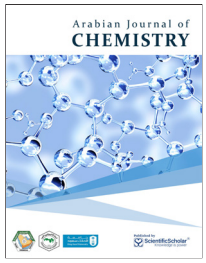

Original Article

High activity Ni-MoS_{2-x} monolayer nano-sheets fabricated through photo-deposition for highly efficient HER in acid solution

Yongling Du[a,*], XuanYe Du[a], Yunmin Du[a], Xiaolong Li[a], Yuhao Li[a], Xuezhao Shi[a], Zhixiang Zheng[b,*]

[a]College of Chemistry and Chemical Engineering, Lanzhou University, Tianshui Road 222, Lanzhou, 730000, Gansu, China
[b]Key Laboratory of Evidence Science Techniques Research and Application of Gansu Province, Gansu University of Political Science and Law, Anning Road 6, Lanzhou, 730070, Gansu, China

ARTICLE INFO

Keywords:
Hydrogen evolution
MoS2 single monolayer
Ni doping MoS2
Photochemical deposition

ABSTRACT

A highly active and stable electro-catalyst for hydrogen evolution was developed by in-situ photo-deposition of Ni metal on MoS_2 nano-sheets with many sulfur vacancies. It was found that Ni metal deposition improved the electrical conductivity of MoS_2 and further enhanced the catalytic activity by synergistic effect with Ni metal with MoS_2 nano-sheets. During photochemical deposition, photo-corrosion moved some sulfur, leading to many sulfur vacancies. Sulfur vacancies further enhance the activity of MoS_2 nano-sheets. Electrochemical experiments demonstrate that the catalyst exhibited excellent hydrogen evolution reaction activity with a large cathode current and a Tafel slope as small as 81 per decade. The high hydrogen evolution activity of Ni-doped MoS_2 was attributed to synergistic electro-catalytic effects between MoS_2 nano-sheets and Ni ions.

1. Introduction

Hydrogen gas has been considered a clean energy source because modern society confronts energy deficits and environmental pollution. Electrochemical-catalytic hydrogen production in an acid solution is one of the most effective and reliable pathways [1-5]. There is no doubt that platinum and its alloys are the most efficient catalysts for hydrogen production. However, the high cost and low reserves have limited their utilization in water electrolysis. Therefore, searching for alternative earth-abundant materials and decreasing the cost of catalysts remain crucial tasks [6-18]. Transition metal disulfides (MS_2) have been considered an up-and-coming alternative to platinum due to their abundance, low cost, and considerable catalytic activity [19-21]. Norskov's group calculated the hydrogen binding energy of MoS_2 and found it was like that of platinum. However, the catalytic activity of 2D MoS_2 was contributed to by its edge sites and sulfur vacancies, leaving many basal plane domains inert for Hydrogen electrochemical revolution (HER) [22]. The HER activity of MoS_2 correlated with the number of catalytically active edge sites and sulfur vacancies that generated new gap states near the Fermi level for hydrogen binding [21,23,24]. As a result, nano-sized MoS_2 is more active than the bulk form due to more exposed sulfur edge sites [25,26]. Based on this understanding, various strategies have been developed to synthesize nano-structured MoS_2 with more defects to improve the HER [6,16,27]. Xie Yi found that the involved oxygen atom can effectively regulate the electronic structure of MoS_2 nano-sheets, enhancing conductivity and HER performance [6]. Zhou Yao *et al.* synthesized Rh-tin-MoS_xO_y. Electron-rich tin prefers to stabilize the unstable optical O site in MoS_xO_y, while Rh is a charge regulator, and oxygen in MoSxOy provides more activation sites. The triple enhancement effect makes Rh-Sn-MoS_xO_y have high electrochemical activity [28]. Using transition metal atoms, such as Ni, Co, Fe, Zn, and Mn-doped MoS_2 nano-sheets, could significantly improve the electrochemical activity of MoS [29-34]. Wang *et al.* demonstrated that the exchange current density of MoS_2 can be increased by incorporating transition metal atoms [33]. Activating the MoS_2 basal plane could improve its HER activity compared to growing edge sites. Hong Li *et al.* used Ar plasma to activate the MoS_2 basal plane by increasing sulfur vacancies to increase MoS_2 catalytic activity [23]. By doping with other transition metal sulfides, such as NiS, MnS, ZnS, and CoS, MnS could improve the HER activity of MoS_2 electro-catalysts [35-39].

Herein, we report a novel photochemical strategy to activate MoS_2 monolayer nanosheets' electrocatalytic activity through NiS-incorporated MoS_2 nanosheets and increased sulfur vacancies. Linear sweep voltammetry and Chronoamperometry were used to study the electrochemical activity of MoS_2 nanosheets and Ni-doping MoS_{2-x} nanosheets. Ni displaced some of Mo through photochemical deposition to form the Ni-S band, which had higher electrochemical activity for hydrogen production. Ni dopant and S defects made Ni-doped MoS_2 monolayer nanosheets have higher catalytic activity for HER.

2. Materials and Methods

2.1. Materials

Single MoS_2 nanosheets were purchased from Jiangsu Xianfeng Nanomaterial Technology Co., Ltd. Nickel nitrate and methanol analytical reagents came from Shanghai Aladdin Biochemical Technology Co., Ltd. H_2SO_4 was purchased from Tianjin Kemiou Chemical Reagent Co., Ltd. The high-purity water was treated through the Ake water system.

*Corresponding authors:
E-mail addresses: duyl@lzu.edu.cn (Y. Du); dqzhenghao@163.com (Z. Zheng)

Received: 17 December, 2024 **Accepted:** 05 March, 2025 **Epub Ahead of Print:** 10 April 2025 **Published:** 17 April 2025
DOI: 10.25259/AJC_283_2024

2.2. Synthesis of catalysts

Typically, 15 mg MoS_2 monolayer nanosheets were dispersed in a 15 mL ethanol solution through ultrasonication. Then, nickel nitrite and 15 mL of pure water were added to the above solution. 0.1 M NaOH and 0.5M H_2SO_4 solution were used to adjust the pH value of the above mixture solution. The MoS_2 nanosheets with different pH values were then illuminated under a 300W Xe light with a 530 nm optical filter for 1 h. The product was washed with a 1:1 ethanol-water solution several times and dried by vacuum cooling drying.

2.3. Preparation of catalyst electrode

Typically, 2 mg of Ni-doping MoS_2 nanosheets catalyst and 30 μL of 0.5% Nafion 717 were dispersed in 1 mL of water by ultrasonication to form a uniform mixture. The catalyst slurry (4 μL) was dropped onto a pure Glass carbon electrode (GCE). Subsequently, a desicator was used to dry the catalyst-modified GCE at room temperature.

2.4. Electrochemical measurements

Electrochemical measurements were performed through a CHI 660C working station with a standard three-electrode cell. The Ni-MoS_2-modified GCE electrode acted as a working electrode, a Pt electrode as an auxiliary electrode, and a saturated calomel electrode (SCE) as a reference electrode. The electro-catalytic activity of MoS_2 monolayer or Ni doped-MoS_2 was examined through cyclic voltammetry, linear sweep voltammetry, and chrono-amperometry in 0.5M H_2SO_4 solution.

The photochemical deposition experiment was performed in 50 ml reaction tubes with ground glass at room temperature, using a 300W Xe lamp with a 530 nm light filter.

2.5. Characterization

An X-ray diffractometer recorded X-ray diffraction (XRD) patterns. Images were collected using a JEM-2100 transmission electron microscope (TEM). X-ray photoelectron spectroscopy (XPS) was studied to confirm the chemical composition of MoS_2 nanomaterials and nickel-doped MoS_2 nanomaterials. The sample of nickel doping MoS_2 nanosheets (Scanning electron microscope (SEM), XPS, and XRD studied) was prepared with the ratio of MoS_2 to Nickel ions (0.8:1) at a pH value of 2.0.

3. Results and Discussion

3.1 Morphology and structure analysis of MoS_2 and Ni doping MoS_2

The XRD pattern of nickel-doping MoS_2 nanosheets and pure MoS_2 nanosheets were studied to assess their crystal structures. The XRD pattern of MoS_2 nanosheets in Figure 1 revealed the characteristic diffraction of 2H-MoS_2 (JCPDS:73-1508). In contrast, no metallic nickel or nickel oxide diffraction was detected in the sample of nickel-doping MoS_2 nanosheets, confirming the presence of a small amount of nickel

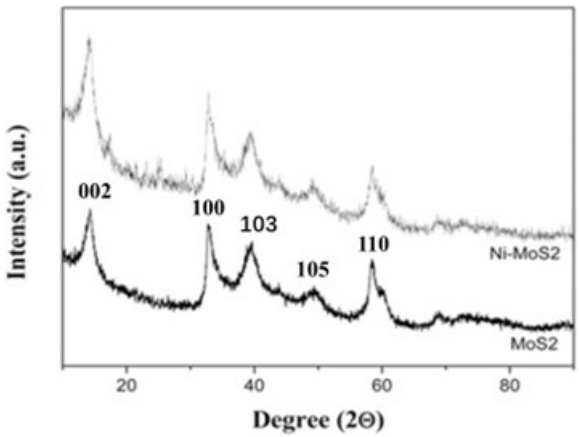

Figure 1. XRD image of MoS_2 nanosheets and Ni doping MoS_2 nanosheets. XRD: X-ray diffraction.

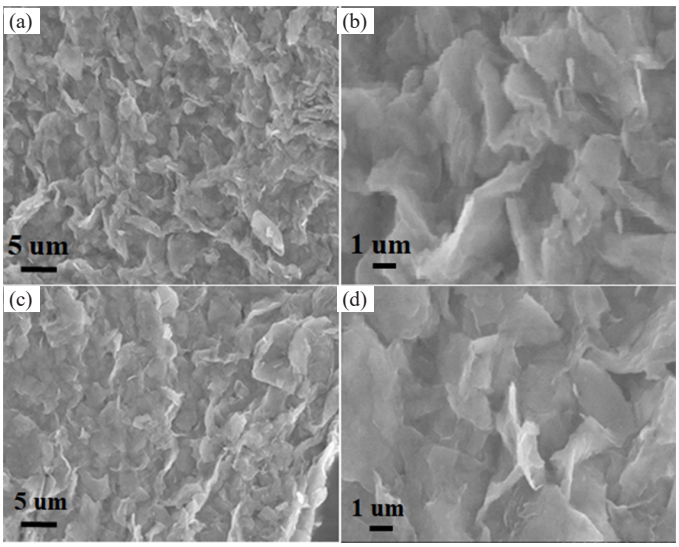

Figure 2. (a) SEM image of MoS_2 nanosheets and (b) enlarged image of MoS_2 nanosheets, (c) SEM image of Ni doping MoS_2 nanosheets and (d) enlarged image of Ni doping MoS_2 nanosheets. SEM: Scanning electron microscope.

in the nickel-doping MoS_2 nanosheets. SEM and TEM characterized the MoS_2 nano-sheet and Ni metal-doped MoS_2 nano-sheet morphology. It can be seen in the SEM image in Figure 2 that there is no significant difference between the pure MoS_2 nano-sheets and Ni-doped MoS_2 nano-sheets. The MoS_2 nano-sheet was larger than 1 μm in both pure MoS_2 nanosheets and nickel-doping MoS_2 nanosheets.

The MoS_2 nanosheets in Figure 3(a) present a folded nano-sheet-like structure, and the morphology of NiS-doped MoS_2 in Figure 3(b) also presents folded nanosheets with some small particles attached to the surface, which may be attributed to NiS produced by the photo-deposition process. High resolution transmission electron microscope (HRTEM) of the MoS_2 nanosheets in Figure 3(c) presents a clear and coherent lattice structure. Many tiny particles are scattered on the

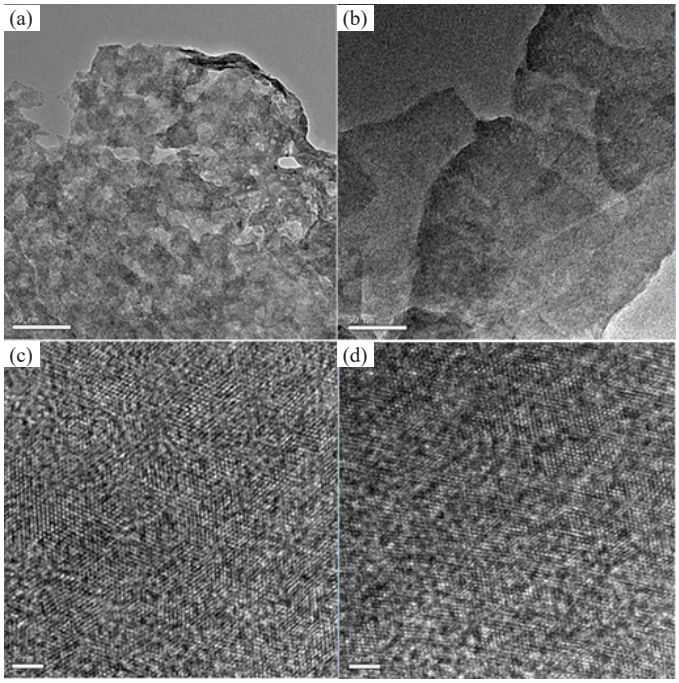

Figure 3. The MoS_2 nanosheets in (a) present a folded nano-sheet-like structure, and the morphology of NiS-doped MoS_2. (b) Presents folded nanosheets with some small particles attached to the surface, which may be attributed to NiS produced by the photo-deposition process. (c-d) HRTEM of the MoS_2 nanosheets (c) presents a clear and coherent lattice structure, (d) with a lattice structure different from the lattice structure of MoS_2, which are NiS particles formed during the photochemical deposition process. HRTEM: High resolution transmission electron microscope.

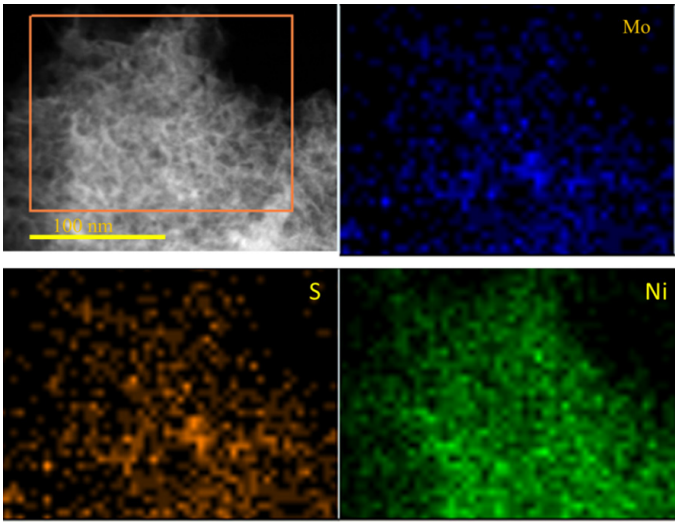

Figure 4. EDX mapping of elements in Ni-doping MoS_{2-x} nano-sheets.

surface of MoS_2 nanosheets in Figure 3(d) with a lattice structure different from the lattice structure of MoS_2, which are NiS particles formed during the photochemical deposition process. This phenomenon, which showed that Ni-doped MoS2 nano-sheets had little difference from pure MoS_2 nano-sheets, could contribute to that small amount of Ni doping in the Ni-MoS_2. The SEM and XRD images had the same phenomena as the TEM images, further confirming the small amount of nickel in Ni-MoS2 nano-sheets.

To further study that Ni had inserted into MoS_2 nano-sheets, the EDX mapping method was used to study the Ni further doping MoS_2 monolayer nano-sheets fabrication. EDX mapping in Figure 4 showed the homogenous distribution of Mo, S, and Ni elements, further confirming that the Ni doping MoS_2 nano-sheet was successfully fabricated using photo-chemical deposition. The EDX and EDX mapping in Figure 4 confirmed that nickel had successfully inserted into MoS_2 nano-sheets.

The Mo, Ni, and S chemical states in the Ni-doped single nanosheets are analyzed using the X-ray photoelectron spectroscopy technique (XPS). The 232.2 and 229 eV peaks belong to Mo 3d 3/2 and 3d 1/2 binding energies (Figure 5a), respectively, which were constant with the structure of MoS_2 nanosheets. The peak (223) belongs to MoO_2, and the binding energy located at 232 belongs to molybdic acid, formed by MoS_2 oxidized by photochemical corrosion. There are also

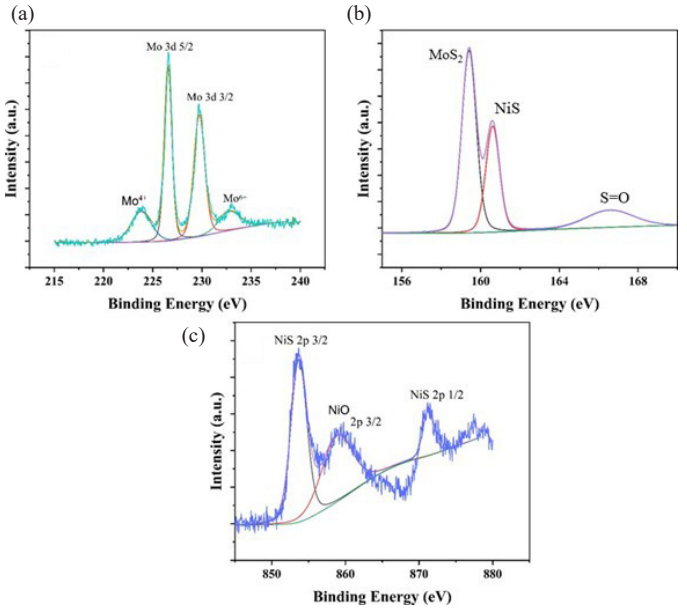

Figure 5. XPS image of (a) Mo 3d, (b) S 1s, and (c) Ni 2p in Ni doping MoS_2 nanosheet. XPS: X-ray photoelectron spectroscopy.

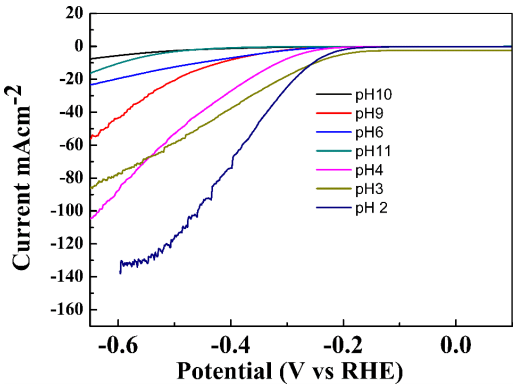

Figure 6. Linear sweep scan image of Ni-MoS_2 in 0.5M H_2SO_4 at a scan rate of 20 mV/s (fabricated in different pH values).

three pairs of characteristic peaks belonging to S elements. The 159.4, 160.6, and 166.6 eV peaks in Figure 5(b) contributed to MoS_2, NiS, and S partly oxidizing, respectively. The electronic valence state of nickel in the above materials was also studied by XPS spectroscopy, with the peak located at 857.8, 871.2 eV in Figure 5(c) contributing to Ni 2p 2/3 and 2p 1/2. Meanwhile, the peak located at 859.1 belongs to nickel oxide. The XPS image research confirms that the Ni-doped MoS_2 nanosheets contain Ni, Mo, and S elements. Nickel exists in the form of nickel sulfide in nickel-doped molybdenum disulfide materials. Like molybdenum disulfide, NiS has good electro-catalytic activity for hydrogen production. The synergistic effect of NiS and MoS_2 gives Ni-MoS_2 higher electrocatalytic activity for hydrogen production.

3.2 Electrochemical performance

3.2.1 pH value affects the catalyst activity

MoS_2 monolayer nanosheets have been widely studied in the electrocatalytic hydrogen reaction. Still, due to their activity, they only originated from edge sites and sulfur vacancies, leaving a tremendous amount of in-plane domains inert. To enhance the catalytic activity of MoS_2 nanosheets, the photochemical method was used to fabricate Ni metal-doped MoS_2 nanosheets. Furthermore, some sulfur atoms were moved by the photochemical corrosion reaction during the photochemical reaction. Subsequently, Ni-doped MoS_2 with many sulfur vacancies has super catalytic activity in hydrogen production.

The pH value of the synthesis environment has dramatically affected the activity of the catalyst. It can be seen in Figure 6 that the pH value has significantly impacted the electro-catalytic activity of Ni-MoS_2. When the pH value decreased from 11 to 2, the electro-catalytic activity of Ni-MoS_2 increased with the pH value decreased. When the pH value was 2, the electrochemical activity got the highest value. pH value has dramatically impacted the activity of Ni-doped MoS_2 nano-sheets for Ni metal deposition, which has been significantly affected by the pH value for hydrogen ions participating in Ni-doped MoS_2 nano-sheet fabrication.

3.2.2 The possible mechanism of Ni-MoS_2 fabrication by photochemical deposition

Ni ions were unstable in the alkaline solution, almost wholly changing into $Ni(OH)_2$. Under the photochemical system, there is a reversible process of Ni ions and $Ni(OH)_2$. The Ni ions were reduced to Ni metal on the surface of the MoS_2 nano-sheet by following the chemical Eqs. (1) to (3):

$$2MoS_2 \xrightarrow{light} MoS_2(hole) + MoS_2(e^-) \quad (1)$$

$$Ni^{2+} + 2MoS_2(e^-) = Ni - MoS_2 + MoS_2 \quad (2)$$

$$2MoS_2(\text{hole}) + CH_3CH_2OH = 2MoS_2 + CH_3CHO + H_2O \quad (3)$$

At the same time, some of part of MoS_2 nano-sheets were decomposed by the following photochemical reaction (Eq. 4):

$$MoS_2 + 14MoS_2(hole) + 8H_2O \rightarrow H_2MoO_4 + 2SO_2 + 14MoS_2 + 14H^+ \quad (4)$$

Some molybdenum ions in the solution had reacted with oxygen to form molybdenum oxide, and other molybdenum ions dissolved in the solution as molybdic acid.

In the basement of the photochemical reaction, Ni metal was reduced by electrons, which were produced by light illumination on MoS_2 nano-sheets to make holes and electrons. The holes were depleted by hole receptor ethanol. The Ni metal kept being deposited until the Ni ions were transferred to NiS and NiO or the light was suddenly shut down.

Under weak acid solution, Ni-MoS_{2-x} was formed through chemical Eqs. (1)-(3). However, under an acid environmental system, the corrosion of MoS_2 would become serious for hydrogen ions to take part in the corrosion process, as shown in the following Eqs. (5)-(7). The nickel metal cluster or nickel oxide particles were unstable and could be dissolved in a robust acid solution. With strong photo-corrosion, many molybdenum or Sulphur lose and leave many active sites; the Ni ions could be coordinated with S and form a Ni-S bond. So, nickel ions were inserted into the structure of MoS_2 and displaced some of the Mo element. The XRD image (Figure 1) of Ni-MoS_2 nano-sheets and MoS_2 nano-sheets had no difference, which confirmed that nickel doping was not only mixed with nickel metal or nickel oxide.

$$14MoS_2(hole) + 8H_2O \rightarrow H_2MoO_4 + 2SO_2 + 13MoS_2 + 14H^+ \quad (5)$$

$$Ni - MoS_2 + 2H^+ = Ni^{2+} + +MoS_2 + H_2 \quad (6)$$

$$Ni^{2+} + 2MoS_2 = Ni - S - MoS_2 + Mo^{2+} \quad (7)$$

During the photochemical deposition, some Ni-S or MoS_2 decomposed to ions and then combined with oxygen to form NiO, MoO_2, and molybdic acid. The Ni-S, NiO, MoO_2, and molybdic acid could enhance MoS2's electrochemical activity. Compared to the high amount of NiS, NiO, MoO_2, and molybdic acid are lesser. A small amount of transition metal, transition sulfide, or transition oxide doping in MoS_2 could enhance the electrocatalytic activity of MoS_2 [37,38,40-43]. The existence of NiS, NiO, MnO_2, and molybdic acid in Ni doping MoS2 nanosheets gives the Ni doping MoS_2 nanosheets a higher electrocatalytic activity than pure MoS_2 nanosheets. The hydrogen ions taking part in photochemical corrosion and Ni-MoS_2 dissolution made a significant amount of MoS_2 decomposed, which led to the lower yield of Ni-MoS_{2-x}.

3.2.3 Electrochemical hydrogen evolution research

Electrochemical hydrogen evolution reactions were studied with different amounts of Ni to Ni-MoS_{2-x} and pure MoS_2 nano-sheets in 0.5M H_2SO_4 solution. Linear sweep voltammetry studies at a scan rate of 20 mv/s exhibit the current density as a function of applied potential. Figure 7 shows that pure MoS_2 exhibited great over-potential value and low current density, contributing to low edge concentration and poor conductivity. In comparison, all the Ni metal doping MoS_{2-x} nano-sheets possessed much lower onset over-potentials than the pure MoS_2 nano-sheets. When the Ni to Mo molar rate was 3.2, the current was 80 mA cm^{-2}, eight times larger than a pure MoS_2 nano-sheet. Under optimized synthesis conditions, the amount of Ni affected the electrochemical activity of the catalyst's HER. When the molar rate of Ni ions to MoS_2 was 0.80, the current of Nickel -MoS_{2-x} was 320 mA cm^{-2}, almost 32 times bigger than pure MoS_2. Under optimized conditions, the over-potential of Ni-MoS_2 was smaller than 100 mV. This phenomenon was relevant to the complication of photochemical deposition. The photochemical deposition is always accompanied by photo-corrosion. Photo-corrosion would lead to S and Mo loss, which would result in more sulfur vacancies and further enhance the MoS_2 catalyst's activity. The higher electrochemical activity of Ni-doping MoS_{2-x} could be attributed to the following reasons: photo-deposition corrosion left many S vacancies and defects, which enhanced HER activity. Ni doping further increased the HER activity of MoS_2. In all, Ni doping and photo-deposition method in acid circumstances made NiS-MoS_{2-x} have higher HER activity. The existence of NiO, MoO_2 and molybdic acid on MoS_2 further enhances the electrochemical activity for hydrogen production. The anisotropic factor of 2D nanomaterials towards their catalytic performance is demonstrated in the active edges.

The polarization curves were also measured in 0.5M H_2SO_4 electrolyte with a scan rate of 20 mv/s, as shown in Figure 8(a). To evaluate the electrochemical activity of Ni-MoS_2, the HER activity of the commercial Pt/C acted as a reference for assessing Ni-MoS_2 performance. Undoubtedly, the Pt/C electro-catalyst exhibits the best electrochemical activity for HER with nearly zero over-potential. The electrochemical activity of H-MoS_2 was poor, with the highest over-potential. The electrochemical activity of Pt-MoS_2 is better than that of MoS_2 nano-sheets, and its over-potential is lower than that of pure MoS2, which means that noble Pt has excellent catalytic activity. Tafel slope is often utilized to evaluate the catalyst's performance, and the smaller Tafel slope means a faster increase in the HER rate with a decrease in over-potentials. The results of the Tafel slope of MoS_2 nano-sheets in Figure 8(b) is 294 mV Dec^{-1}, which matches several earlier reports for MoS_2 nano-sheet catalysts. The Tafel slope of Ni doping MoS_{2-x} is 81 mV decade-1, which is almost as good as Pt/C. To reach the current density of 10 mA cm^{-2}, the reference point, the over-potential of -300mv, is required for the pure MoS_2. Compared with pure MoS_2, the over-potential is only -200mv for the Ni-doped MoS_{2-x} monolayer nano-sheets.

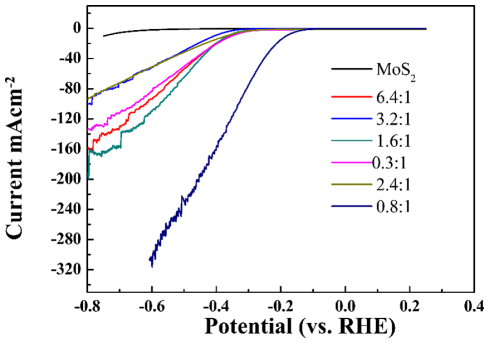

Figure 7. LSV image of Ni-MOS_{2-x} in 0.5M H_2SO_4 solution fabricated with different ratios of Ni ions compared with MoS_2 at a scan rate of 20 mV/s.

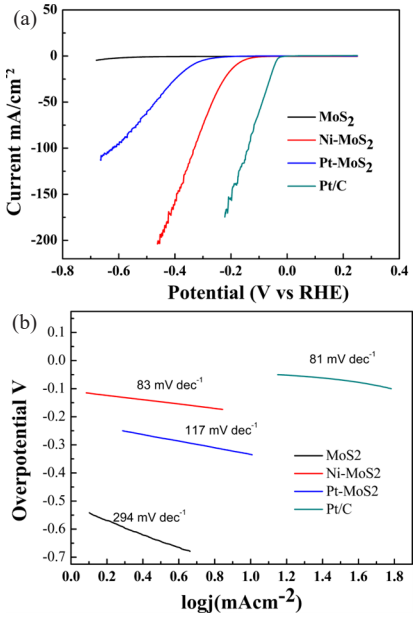

Figure 8. (a) Polarization curves of different electrodes at a scan rate of 20 mV/s. (b) Tafel plots of different materials modified electrodes.

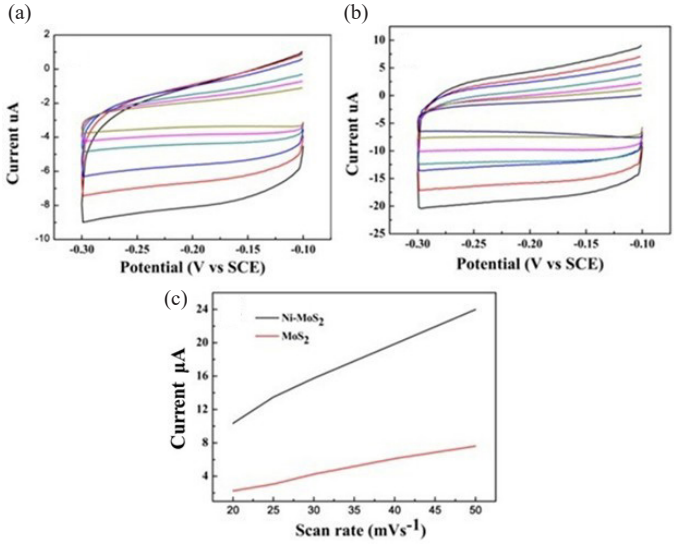

Figure 9. (a) Cyclic voltammetry of MoS_2 nanosheets modified GCE in 0.5M H_2SO_4 at different scan rates. (b) Cyclic voltammetry image of Ni-MoS_2 modified GCE in 0.5M H_2SO_4 at different scan rates. (c) Capacitive currents over nickel doping MoS_2 nanosheets and pure MoS_2 nanosheets vs scan rate. GCE: Glass carbon electrode.

To initiate HER in the acid electrolyte, three principal steps would involve H^+ to H_2, which contain the Volmer equation, Herrovsky equation, and Tafel reaction equation. The Ni-MoS_2 nano-sheets exhibit a Tafel slope of 83 mv/dec, which is lower than pure MoS_2 (294 mv/dec) and Pt-MoS_2 (197 mv/dec) nano-sheets. The Ni-MoS_2 is almost as super as Pt/C (81 mv/dec), which gives them great potential in electrochemical hydrogen production. The Tafel plot of Ni-MoS_2 nano-sheets is shallow, meaning that the electrochemical reaction on the surface of Ni-MoS_2 proceeds through the Volmer-Herrvosky mechanism step.

The electrochemical capacitance surface area measurements were also researched to study the electrochemical active area of MoS_2 and Ni-MoS_2 nano-sheets. The electrochemical double layer charge of MoS_2 and Ni single atom doped MoS_2 were measured. As shown in Figure 9(a) and 9(b), the capacitive current of Ni-doped MoS_2 nano-sheets is more significant than that of pure MoS_2 nano-sheets at the scan rate of 40mv/s. Fig exhibits that the calculated capacitive current of Ni-MoS_2 is more significant than pure MoS_2. Figure 9(c) displays the measured capacitive currents plotted as a function of scan rate, and it also reveals that Ni-doped MoS_2 shows a larger double-layer capacitance than pure MoS_2 nano-sheets, which further confirmed that Ni-doping MoS_2 nano-sheets had high catalytic activity than pure MoS_2 nano-sheets.

Stability is another essential criterion used to evaluate the catalyst's HER activity. Continuous HER at a given over-potential was conducted to explore the durability of the Ni-doped MoS_2 nano-sheets in a 0.5M H_2SO_4 environment. As shown in Figure 10(a), the stability of the cathodic current of Ni-MoS_2 is higher than 10 $mAcm^{-2}$, which is five times higher than pure MoS_2. The 2H-MoS_2 can act as HER catalyst,

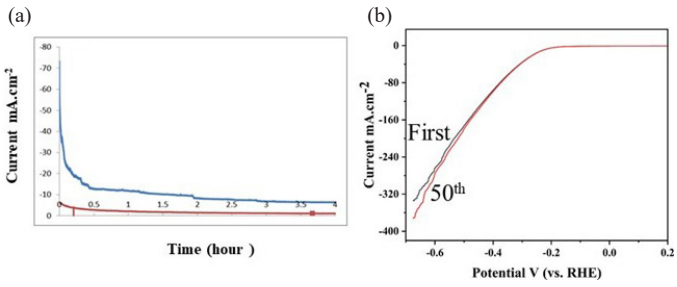

Figure 10. (a) Stability test at the fixed potential of -1.0 vs. SCE in 0.5M H_2SO_4 solution (blue line: Ni-MoS_2 nano-sheets, red line: pure MoS_2 nano-sheets), (b) Stability of nickel doping MoS_2 nanosheets modified electrode by LSV methods. SCE: Saturated calomel electrode.

and the hydrogen evolution reaction occurred at a higher over-potential than Ni-doped MoS_2 nano-sheets. The doping of Ni into MoS_2 nano-sheets leads to profound enhancements of HER activities. The recycle stability test was also studied through the LSV method in 0.5 M H_2SO_4 solution at a scan rate of 20 mV/s on the nickel doping MoS_2 nanosheet-modified electrode. As shown in Figure 10(b), there is no significant difference between the first scan of LSV of nickel doping MoS_2 nanosheets and the 50th cycle, which further confirms that nickel doping MoS_2 has stable catalytic activity for hydrogen production in acid solution.

4. Conclusions

We fabricated Ni doping MoS_{2-x} nano-sheets using the photochemical method. The electrochemical activity of Ni-MoS_{2-x} was greatly influenced by pH value. The Ni-doped MoS_2 nano-sheets were fabricated using two different photochemical deposition mechanisms: acid and alkaline. The Ni-doped monolayer MoS_2 fabricated in an acid solution with a pH value of 2 had the highest electrochemical activity. The Ni-doped monolayers fabricated in an acid solution were compared in terms of MoS_2 corrosion and Ni deposition, leading to more S defects. Ni was inserted into the structure of MoS_2 to displace some Mo elements. Ni displacement, S defects, NiO, MnO_2, and molybdic acid in MoS_2 made Ni-MoS_{2-x} have the highest activity for hydrogen production in acid solution. This is a new method to fabricate high electro-catalytic nanomaterials with great potential in the hydrogen production industry.

CRediT authorship contribution statement

Yonging Du: Experimental program design, nanomaterial synthesis, electrochemical testing, and manuscript writing; **Xuanye Du**: electrochemical test of MoS_2 nanosheets and NiS-doping MoS_2 nanosheets; **Yunming Du**: stability test of NiS doping MoS_{2-x} and the Figures plotted; **Xiaolong Li:** XRD and XPS test and related data process; **Yuhao Li**: nanomaterials synthesis; **Xuezhao Shi**: English polishing for the manuscript; **Zhixiang Zheng**: Funding supporting.

Declaration of competing interest

The authors declare no competing interest.

Declaration of Generative AI and AI-assisted technologies in the writing process

The authors confirm that there was no use of artificial intelligence (AI)-assisted technology for assisting in the writing or editing of the manuscript and no images were manipulated using AI.

Acknowledgment

This worker was supported by the National Natural Science Foundation of China (No. 51862029), the Industry Support and Guidance Project for Colleges and Universities in Gansu Province in 2020 (No. 2020C-32), Lanzhou Talent Innovation and Entrepreneurship Project (No.2019-RC-99), Key Talent Project of Gansu Province (No. 2022RCXM085).

References

1. Yu, X., Prévot, M.S., Guijarro, N., Sivula, K., 2015. Self-assembled 2D WSe2 thin films for photoelectrochemical hydrogen production. *Nature Communication*, **6**, 7596. https://doi.org/10.1038/ncomms8596
2. Landman, A., Dotan, H., Shter, G.E., Wullenkord, M., Houaijia, A., Maljusch, A., Grader, G.S., Rothschild, A., 2017. Photoelectrochemical water splitting in separate oxygen and hydrogen cells. *Nature Materials*, **16**, 646-651. https://doi.org/10.1038/nmat4876
3. Li, H., Du, M., Mleczko, M.J., Koh, A.L., Nishi, Y., Pop, E., Bard, A.J., Zheng, X., 2016. Kinetic study of hydrogen evolution reaction over strained MoS_2 with sulfur vacancies using scanning electrochemical microscopy. *Journal of the American Chemical Society*, **138**, 5123-5129. https://doi.org/10.1021/jacs.6b01377
4. Huang, Z.F., Song, J., Li, K., Tahir, M., Wang, Y.T., Pan, L., Wang, L., Zhang, X., Zou, J.J., 2016. Hollow cobalt-based bimetallic sulfide polyhedra for efficient all-

pH-value electrochemical and photocatalytic hydrogen evolution. *Journal of the American Chemical Society*, **138**, 1359-1365. https://doi.org/10.1021/jacs.5b11986
5. Perry, S.C., Pangotra, D., Vieira, L., Csepei, L.énárd-I.án, Sieber, V., Wang, L., Ponce de León, C., Walsh, F.C., 2019. Electrochemical synthesis of hydrogen peroxide from water and oxygen. *Nature Reviews Chemistry*, **3**, 442-458. https://doi.org/10.1038/s41570-019-0110-6
6. Xie, J., Zhang, H., Li, S., Wang, R., Sun, X., Zhou, M., Zhou, J., Lou, X.W., Xie, Y., 2013. Defect-rich MoS_2 ultrathin nanosheets with additional active edge sites for enhanced electrocatalytic hydrogen evolution. *Advanced Materials (Deerfield Beach, Fla.)*, **25**, 5807-5813. https://doi.org/10.1002/adma.201302685
7. Valenti, G., Boni, A., Melchionna, M., Cargnello, M., Nasi, L., Bertoni, G., Gorte, R.J., Marcaccio, M., Rapino, S., Bonchio, M., Fornasiero, P., Prato, M., Paolucci, F., 2016. Co-axial heterostructures integrating palladium/titanium dioxide with carbon nanotubes for efficient electrocatalytic hydrogen evolution. *Nature Communication*, **7**, 13549. https://doi.org/10.1038/ncomms13549
8. Alinezhad, A., Gloag, L., Benedetti, T.M., Cheong, S., Webster, R.F., Roelsgaard, M., Iversen, B.B., Schuhmann, W., Gooding, J.J., Tilley, R.D., 2019. Direct growth of highly strained pt islands on branched Ni nanoparticles for improved hydrogen evolution reaction activity. *Journal of the American Chemical Society*, **141**, 16202-7. https://doi.org/10.1021/jacs.9b07659
9. Ma, B., Guan, P.Y., Li, Q.Y., Zhang, M., Zang, S.Q., 2016. MOF-derived flower-like MoS_2@TiO_2 nanohybrids with enhanced activity for hydrogen evolution. *ACS Applied Materials & Interfaces*, **8**, 26794-26800. https://doi.org/10.1021/acsami.6b08740
10. Karunadasa, H.I., Montalvo, E., Sun, Y.J., Majda, M., Long, J.R., Chang, C.J., 2012. A molecular MoS_2 edge site mimic for catalytic hydrogen generation. *Science*, **335**, 698-702. https://doi.org/10.1126/science.1215868
11. Saifi, S., Dey, G., Karthikeyan, J., Sinha, A.S.K., Aijaz, A., 2022. MoS_2 and WS2 nanosheets decorated on metal–organic framework-derived cobalt/carbon nanostructures as electrocatalysts for hydrogen evolution. *ACS Applied Nano Materials* **5**, 10696-10703. https://doi.org/10.1021/acsanm.2c02028
12. Li, Y., Wang, H., Xie, L., Liang, Y., Hong, G., Dai, H., 2011. MoS_2 nanoparticles grown on graphene: an advanced catalyst for the hydrogen evolution reaction. *Journal of the American Chemical Society*, **133**, 7296-99. https://doi.org/10.1021/ja201269b
13. Mohanty, B., Mitra, A., Jena, B., Jena, B.K., 2020. MoS_2 quantum dots as efficient electrocatalyst for hydrogen evolution reaction over a wide pH range. *Energy & Fuels*, **34**, 10268-10275. https://doi.org/10.1021/acs.energyfuels.0c01283
14. Hu, M., Wang, Z., Li, M., Guo, C., Li, L., 2022. Nanosheet MoS_2-decorated MoO2 on porous carbon as electrodes for efficient hydrogen evolution. *ACS Applied Nano Materials*, **5**, 8175-8183. https://doi.org/10.1021/acs.energyfuels.0c01283
15. Wang, S., Li, Y., Hu, Y., Zhou, X., Zhang, M., Jia, X., Yang, Y., Lin, B.-L., Chen, G., 2022. One-step synthesis of 1T MoS_2 hierarchical nanospheres for electrocatalytic hydrogen evolution. *ACS Applied Energy Materials*, **5**, 11705-11712. https://doi.org/10.1021/acsanm.2c01272
16. Wang, X., Zhang, Y., Si, H., Zhang, Q., Wu, J., Gao, L., Wei, X., Sun, Y., Liao, Q., Zhang, Z., Ammarah, K., Gu, L., Kang, Z., Zhang, Y., 2020. Single-atom vacancy defect to trigger high-efficiency hydrogen evolution of MoS_2. *Journal of the American Chemical Society*, **142**, 4298-4308. https://doi.org/10.1021/jacs.9b12113
17. Puente Santiago, A.R., He, T., Eraso, O., Ahsan, M.A., Nair, A.N., Chava, V.S.N., Zheng, T., Pilla, S., Fernandez-Delgado, O., Du, A., Sreenivasan, S.T., Echegoyen, L., 2020. Tailoring the interfacial interactions of van der waals 1T-MoS_2/C60 heterostructures for high-performance hydrogen evolution reaction electrocatalysis. *Journal of the American Chemical Society*, **142**, 17923-27. https://doi.org/10.1021/jacs.0c08867
18. Chandrasekaran, S., Feaster, J., Ynzunza, J., Li, F., Wang, X., Nelson, A.J., Worsley, M.A., 2022. Three-dimensional printed MoS_2/Graphene aerogel electrodes for hydrogen evolution reactions. *ACS Materials Au*, **2**, 596-601. https://doi.org/10.1021/acsmaterialsau.2c00014
19. Huang, S., Jin, Z., Ning, P., Gao, C., Wu, Y., Liu, X., Xin, P., Chen, Z., Jiang, Y., Hu, Z., Chen, Z., 2021. Synergistically modulating electronic structure of niS2 hierarchical architectures by phosphorus doping and sulfur-vacancies defect engineering enables efficient electrocatalytic water splitting. *Chemical Engineering Journal*, **420**, 127630. https://doi.org/10.1016/j.cej.2020.127630
20. Feldman, Y., Wasserman, E., Srolovitz, D.J., Tenne, R., 1995. High-rate, gas-phase growth of MoS_2 nested inorganic fullerenes and nanotubes. *Science (New York, N.Y.)*, **267**, 222-5. https://doi.org/10.1126/science.267.5195.222
21. Voiry, D., Fullon, R., Yang, J., de Carvalho Castro E Silva, C., Kappera, R., Bozkurt, I., Kaplan, D., Lagos, M.J., Batson, P.E., Gupta, G., Mohite, A.D., Dong, L., Er, D., Shenoy, V.B., Asefa, T., Chhowalla, M., 2016. The role of electronic coupling between substrate and 2D MoS_2 nanosheets in electrocatalytic production of hydrogen. *Nature Materials*, **15**, 1003-9. https://doi.org/10.1038/nmat4660
22. Deng, J., Li, H., Xiao, J., Tu, Y., Deng, D., Yang, H., Tian, H., Li, J., Ren, P., Bao, X., 2015. Triggering the electrocatalytic hydrogen evolution activity of the inert two-dimensional MoS_2 surface via single-atom metal doping. *Energy & Environmental Science*, **8**, 1594-1601. https://doi.org/10.1039/C5EE00751H
23. Li, H., Tsai, C., Koh, A.L., Cai, L., Contryman, A.W., Fragapane, A.H., Zhao, J., Han, H.S., Manoharan, H.C., Abild-Pedersen, F., Norskov, J.K., Zheng, X., 2016. Activating and optimizing MoS_2 basal planes for hydrogen evolution through the formation of strained sulphur vacancies. *Nature Materials*, **15**, 364. https://doi.org/10.1038/nmat4465
24. Tsai, C., Li, H., Park, S., Park, J., Han, H.S., Nørskov, J.K., Zheng, X., Abild-Pedersen, F., 2017. Electrochemical generation of sulfur vacancies in the basal plane of MoS_2 for hydrogen evolution. *Nature Communication*, **8**, 15113. https://doi.org/10.1038/ncomms15113
25. Xie, J., Zhang, J., Li, S., Grote, F., Zhang, X., Zhang, H., Wang, R., Lei, Y., Pan, B., Xie, Y., 2013. Controllable disorder engineering in oxygen-incorporated MoS_2 ultrathin nanosheets for efficient hydrogen evolution. *Journal of the American Chemical Society*, **135**, 17881-8. https://doi.org/10.1021/ja408329q
26. Gao, M.R., Chan, M.K., Sun, Y., 2015. Edge-terminated molybdenum disulfide with a 9.4-A interlayer spacing for electrochemical hydrogen production. *Nature Communication*, **6**, 7493. https://doi.org/10.1038/ncomms8493
27. Liu, Q., Fang, Q., Chu, W., Wan, Y., Li, X., Xu, W., Habib, M., Tao, S., Zhou, Y., Liu, D., Xiang, T., Khalil, A., Wu, X., Chhowalla, M., Ajayan, P.M., Song, L., 2017. Electron-doped 1T-MoS_2 via interface engineering for enhanced electrocatalytic hydrogen evolution. *Chemistry of Materials*, **29**, 4738-4744. https://doi.org/10.1021/acs.chemmater.7b00446
28. Zhou, Y., Hao, W., Zhao, X., Zhou, J., Yu, H., Lin, B., Liu, Z., Pennycook, S.J., Li, S., Fan, H.J., 2022. Electronegativity-induced charge balancing to boost stability and activity of amorphous electrocatalysts. *Advanced Materials*, **34**. https://doi.org/10.1002/adma.202100537
29. Shi, Y., Zhou, Y., Yang, D.R., Xu, W.X., Wang, C., Wang, F.B., Xu, J.J., Xia, X.H., Chen, H.Y., 2017. Energy level engineering of MoS_2 by transition-metal doping for accelerating hydrogen evolution reaction. *Journal of the American Chemical Society*, **139**, 15479-15485. https://doi.org/10.1021/jacs.7b08881
30. Sun, T., Wang, J., Chi, X., Lin, Y., Chen, Z., Ling, X., Qiu, C., Xu, Y., Song, L., Chen, W., Su, C., 2018. Engineering the electronic structure of MoS_2 nanorods by N and Mn dopants for ultra-efficient hydrogen production. *ACS Catalysis*, **8**, 7585-7592. https://doi.org/10.1021/acscatal.8b00783
31. Özgür, D.Ö., Özkan, G., Atakol, O., Çelikkan, H., 2021. Facile ion-exchange method for Zn intercalated MoS_2 as an efficient and stable catalyst toward hydrogen evaluation reaction. *ACS Applied Energy Materials*, **4**, 2398-2407. https://doi.org/10.1021/acsaem.0c02899
32. Yu, X.Y., Feng, Y., Jeon, Y., Guan, B., Lou, X.W., Paik, U., 2016. Formation of ni-co-MoS_2 nanoboxes with enhanced electrocatalytic activity for hydrogen evolution. *Advanced Materials (Deerfield Beach, Fla.)*, **28**, 9006-9011. https://doi.org/10.1002/adma.201601188
33. Wang, D., Zhang, X., Shen, Y., Wu, Z., 2016. Ni-doped MoS_2nanoparticles as highly active hydrogen evolution electrocatalysts. *RSC Advances*, **6**, 16656-16661. https://doi.org/10.1039/C6RA02610A
34. Pan, Y., Lin, Y., Liu, Y., Liu, C., 2016. A novel CoP/MoS_2-CNTs hybrid catalyst with Pt-like activity for hydrogen evolution. *Catalysis Science & Technology* **6**, 1611-1615. https://doi.org/10.1039/C5CY02299A
35. Panghal, A., Sahoo, D., Deepak, D., Deshmukh, S., Kaviraj, B., Roy, S.S., 2024. Single-step synthesis of Ni-Doped MoS_2 nanostructures for symmetrical supercapacitor devices. *ACS Applied Nano Materials*, **7**, 5358-5371. https://doi.org/10.1021/acsanm.3c06139
36. Zhao, X., Bao, J., Zhou, Y., Zhang, Y., Sheng, X., Wu, B., Wang, Y., Zuo, C., Bu, X., 2022. Heterostructural MoS_2/NiS nanoflowers via precise interface modification for enhancing electrocatalytic hydrogen evolution. *New Journal of Chemistry*, **46**, 5505-5514. https://doi.org/10.1039/D1NJ05873H
37. Hao, J., Huang, L., Han, S., Lian, J., 2023. MnS-MoS_2 nanosheets supported on Mo plates as electrocatalyst for the hydrogen evolution reaction. *ACS Applied Nano Materials*, **7** (1), 638-648. https://doi.org/10.1021/acsanm.3c04781
38. Ma, C., Zhu, S., Zhao, Y., Wang, X., Zhan, T., Chen, L., Wang, J., Ling, Q., Xiao, Z., Wu, X., Cai, J., Wu, P., 2024. CoS2-MoS_2 nanoflower arrays for efficient hydrogen evolution reaction in the universal pH range. *Langmuir*, **40**, 744-750. https://doi.org/10.1021/acs.langmuir.3c02960
39. Lu, Y., Pei, C., Li, Y., Zhao, Z., Park, H.S., Yu, X., 2024. Boosted electrochemical hydrogen evolution activity via the core-shell heterostructure of nickel sulfide nanoframe-supported layered rhenium disulfide. *ACS Applied Materials & Interfaces*, **16**, 53864-53872. https://doi.org/10.1021/acsami.4c11277
40. Lonkar, S.P., Pillai, V.V., Alhassan, S.M., 2018. Three-dimensional NiS-MoS_2/graphene heterostructured nanohybrids as high-performance hydrodesulfurization catalysts. *ACS Applied Nano Materials*, **1**, 3114-3123. https://doi.org/10.1021/acsanm.8b00287
41. Shi, B.-Y., Li, H.-Y., Cao, H.-X., Zheng, X.-Y., Liu, Y., Yao, C.-B., 2024. Photogenerated Carrier Separation and Localized Surface Plasmon Resonance in MoS_2/Metal Nanocomposites: Implications for Photoelectric Devices. *ACS Applied Nano Materials*, 7, 12806-12820. https://doi.org/10.1021/acsanm.4c01222
42. Ye, S., Du, Z., Cai, Z., Ou, D., Guo, H., Liu, Q., Yang, W., Shi, Q., 2024. Mn-Doped crystalline Ni3S2/AMORPHOUS MoS_2 core-shell nanorods as bifunctional electrocatalysts for highly-efficient overall water splitting. *ACS Applied Nano Materials*, **7**, 3096-3104. https://doi.org/10.1021/acsanm.3c05420
43. Ali Sheikh, Z., Vikraman, D., Faizan, M., Kim, H., Aftab, S., F Shaikh, S., Nam, K.W., Jung, J., Hussain, S., Kim, D.K., 2024. Formulation of hierarchical nanowire-structured coNiO2 and MoS_2/CoNiO2 hybrid composite electrodes for supercapacitor applications. *ACS Applied Materials & Interfaces*, **16**, 10104-10115. https://doi.org/10.1021/acsami.3c17201